First Order Sea Clutter Cross Section for HF Hybrid Sky-Surface Wave Radar

Yongpeng ZHU, Yinsheng WEI, Yajun LI

School of Electronics and Information Engineering, Harbin Institute of Technology, Harbin, 150001, China

zhuyp@hit.edu.cn, weiys@hit.edu.cn, liyajun1985happy@163.com

Abstract. *This paper presents a modified method to simulate the first order sea clutter cross section for high frequency (HF) hybrid sky-surface wave radar, based on the existent model applied in the bistatic HF surface wave radar. The modification focuses on the derivation of Bragg scattering frequency and the ionosphere dispersive impact on the clutter resolution cell. Meanwhile, an analytic expression to calculate the dispersive transfer function is derived on condition that the ionosphere is spherical stratified. Simulation results explicate the variance of the cross section after taking account of the influence triggered by the actual clutter resolution cell, and the spectral width of the first order sea clutter is defined so as to compare the difference. Eventually, experiment results are present to verify the rationality and validity of the proposed method.*

Keywords

Clutter resolution cell, ionosphere dispersion, first order sea clutter cross section, HF hybrid sky-surface wave radar.

1. Introduction

The HF hybrid sky-surface wave radar is a novel radar configuration, which consists of the sky wave transmitting and surface wave receiving propagation path, and the basic schematic diagram of the detection principle is illustrated in Fig. 1. Such special hybrid travelling channel not only maintains the capacity of detecting targets over the horizon, but also makes the deployment of receiving antenna array much more flexible [1], [2].

However, the ocean surface, as the primary medium of ground wave diffraction, brings in the issue of sea clutter interference at the same time. Now that the sea clutter, especially the first order sea clutter, constructs the major detection background of targets with low Doppler frequency [3]-[5], therefore it is worthwhile to comprehend the characteristic of which so as to enhance the detection probability of targets [6]-[10]. Therefore, the radar cross section (RCS) model has been studied afterwards to simulate the first and second order RCS of the sea clutter applicable in the monostatic and bistatic HF surface wave radar

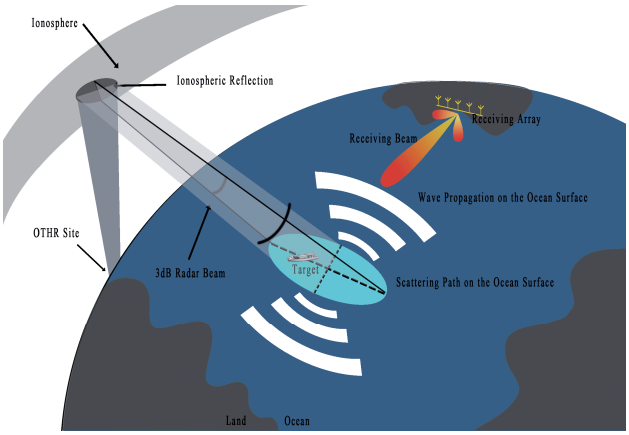

Fig. 1. The detection principle diagram of HF hybrid sky-surface wave radar.

(HFSWR) [11], [12]. However, given the hybrid propagation mode herein, the travelling path consists of the ionosphere reflection. Therefore, in order to explicate the ionospheric influence on the clutter cross section, we mainly focus on its influence on the clutter resolution cell A_c as a matter of fact that the normalized radar cross section denoted by the symbol σ^0 is given as $\sigma^0 = \sigma_c/A_c$ [13], where σ_c is the radar cross section of clutter occupying A_c. While, the effect on the clutter resolution cell imposed by ionosphere is an important problem that is to mention but a few. As far as the existing published analysis [14], [15], the ionospheric dispersive feature is regarded as the princeps factor leading to this. In order to explain the ionosphere dispersion, Lundborg [14] has derived an analytical expression of the ionosphere dispersive transfer function under the assumption that the ionosphere is plane stratified and the electron density profile obeys the parabolic model.

Besides, such new travelling path also introduces a number of new arguments such as the grazing angle and the lateral scattering angle etc. Therefore, a redefined formula to calculate the Bragg scattering frequency appears to be an issue worthy of study in the HF hybrid sky surface wave radar after taking account of these variable effects.

Given these key problems aforementioned, the paper is set out as follows. Section 2 focuses on the derivation of the Bragg scattering frequency accommodating to this hybrid propagation system. Section 3 explains the effect on the clutter resolution cell resulting from ionosphere disper-

sion property. In this section, we consider the case of spherical geometry gaining simplicity by neglecting the influence of the geomagnetic field and collisions. The expression of dispersive coefficient, a critical argument determining the dispersive transfer function, is derived in Appendix A, which is appropriate for a spherical stratified ionosphere and quasi-parabolic (Q-P) model. Section 4 simulates the radar cross section of the first order sea clutter after taking the influence of clutter resolution cell into consideration. Furthermore, experiment results are provided to verify the effectiveness of the simulation method. Eventually, our results are summarized in Section 5.

2. Derivation of Bragg Scattering Frequency

2.1 Spatial Geometry Distribution of the First Order Sea Clutter

HF sky-surface wave radar makes use of the sky wave radar station located inland as a transmitting station, monitoring the ocean area of interest through ionosphere reflection, and finally the backscattered echo is received by the shore-based receiver by means of diffraction on the ocean surface. A simplified propagation path can be seen in Fig. 2, where the symbol *Tr* and *Rr* indicate the position of transmitter and receiver, respectively. *T* is another ellipse focus relative to *Rr* .

As the time delay corresponds to the distance between the target and the receiver given the conventional radar signal processing, it is reasonable to take it as an independent variable to deduce the distribution of the first order sea clutter. Firstly, combined with the geometry relationship, we could obtain the following equations easily assuming that the ionosphere is not inclined, viz. $R_1 = R_2$

$$R_1^2 = h^2 + (R_t / 2)^2 , \tag{1}$$

$$R_t^2 = D_0^2 + R^2 - 2D_0 R\cos\theta_r , \tag{2}$$

$$d = R_1 + R_2 + R = 2R_1 + R . \tag{3}$$

Based on (1) – (3), the target location can be expressed as

$$R = \frac{d^2 - 4h^2 - D_0^2}{2d - 2D_0\cos\theta_r}$$

where D_0 indicates the baseline distance between the transmitting and receiving stations; d is the group range which could be estimated by the time delay; R is the distance from the target to the receiving station; θ_r is the angle between R and the baseline; h represents the ionospheric reflection height; Δ_i is the grazing angle.

Afterwards, the group range d is postulated to be fixed, which is equivalent to make the time delay invariant and then the coordinates could be constructed as follows:

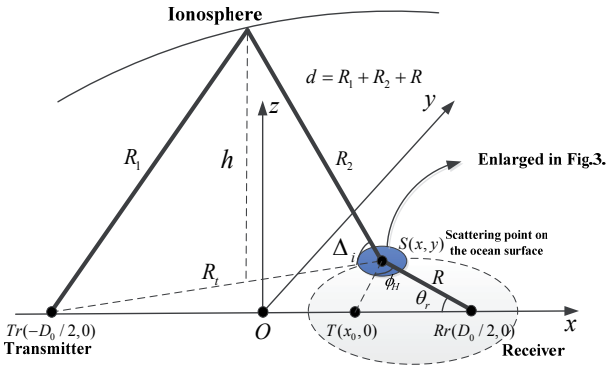

Fig. 2. Hybrid sky-surface propagation channel illustration (solid bold line) and the ellipse trajectory distribution of the sea clutter (dotted line) corresponding to a fixed time delay.

The baseline is x axis, the normal direction is y axis and the central point O is the origin; therefore, we have the following mathematical relationship

$$\begin{cases} (x + \dfrac{D_0}{2})^2 + y^2 = (2h\cot\Delta_i)^2 \\ (x - \dfrac{D_0}{2})^2 + y^2 = R^2 \end{cases}$$

Therefore, the coordinate (x, y) of the scattering point S on the ocean surface could be easily obtained by

$$\begin{cases} x = \dfrac{(2h\cot\Delta_i)^2 - R^2}{2D_0} \\ y = \pm\sqrt{(2h\cot\Delta_i)^2 - (x + D_0/2)^2} \end{cases} \tag{4}$$

Furthermore, based on (4), we figure out that the locus of S could also be described as an ellipse equation (the dashed line in Fig. 2.) with the focus $T(x_0, 0)$ and $Rr(D_0/2, 0)$.

$$(x - x_c)^2 / a^2 + y^2 / b^2 = 1 , \tag{5}$$

$$a = \frac{(d^2 - 4h^2 - D_0^2)d}{2(d^2 - D_0^2)} , \quad c = \frac{(d^2 - 4h^2 - D_0^2)D_0}{2(d^2 - D_0^2)} , \tag{5a}$$

$$b = \sqrt{a^2 - c^2} , \qquad x_c = \frac{2h^2 D_0}{d^2 - D_0^2} . \tag{5b}$$

The corresponding parameters are obtained by (5a)–(5b), and the detailed derivation is not stated herein for the sake of the article length.

2.2 Derivation of the Sea Wave Vector Responsible for Bragg Scattering

Given the relationship between the incident wave vector and scattering wave vector illustrated in Fig. 3, the sea wave vector responsible for Bragg scattering could be regarded as the composition output of vectors. Furthermore,

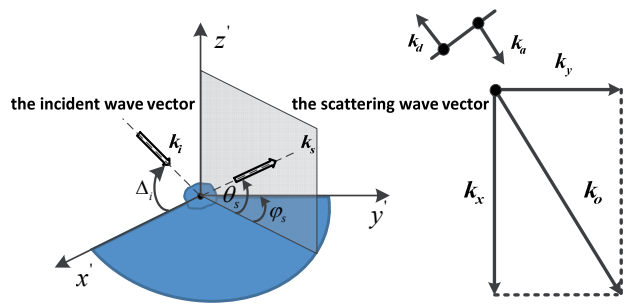

Fig. 3. Geometry for scattering from the patch on the ocean surface.

according to Fig. 3, the elementary scattering relationship could be expressed as

$$\boldsymbol{k}_x = \boldsymbol{k}_s \cos\theta_s \sin\varphi_s + \boldsymbol{k}_i \cos\Delta_i , \tag{6}$$

$$\boldsymbol{k}_y = \boldsymbol{k}_s \cos\theta_s \cos\varphi_s , \tag{7}$$

$$\boldsymbol{k}_o = \boldsymbol{k}_x + \boldsymbol{k}_y . \tag{8}$$

In Fig. 3, the ascending wave vector $\boldsymbol{k}_a$ and the descending wave vector $\boldsymbol{k}_d$ responsible for the positive and negative Bragg scattering frequency can be interpreted as in the same and opposite direction of $\boldsymbol{k}_o$. In addition, since the velocity v of a sea wave of length L is given by $v = \sqrt{gL/(2\pi)}$ [11] and the sea wave number k_0 is determined by $k_0 = 2\pi / L$, the intrinsic frequency for a particular sea wave can be obtained by (9), based on the assumption that the absolute value of the wave vector before and after scattering keeps equal, viz. $|\boldsymbol{k}_i| = |\boldsymbol{k}_s| = k$.

$$\begin{aligned}\omega_H &= 2\pi f_H = 2\pi v / L \\ &= \frac{2\pi}{L}\sqrt{\frac{gL}{2\pi}} = \sqrt{gk_0} \\ &= \sqrt{gk}\left(\cos^2\Delta_i + \cos^2\theta_s + 2\cos\theta_s \sin\varphi_s \cos\Delta_i\right)^{1/4}\end{aligned} \tag{9}$$

Actually, strong scattering happens once the sea wave intrinsic vibrating frequency resonates with the radar radio wave frequency. And the resonating frequency ω_H is regarded as in consistence with Bragg scattering frequency [11]. Furthermore, θ_S in Fig. 3 equals to zero since the radar radio wave received by the receiver is diffracted on the ocean surface. And compared with the geometry relationship in Fig. 2 and Fig. 3, it is easy to yield the result that $\varphi_s = \theta_r$. Therefore, equation (9) could be simplified as

$$\omega_H = \sqrt{gk}\left(\cos^2\Delta_i + 1 + 2\sin\theta_r \cos\Delta_i\right)^{1/4} . \tag{10}$$

Besides, allowing for the fact that the spatial geometry distribution of the first order sea clutter in bistatic HFSWR could be described by an ellipse [12], the result of which is also consistent with the conclusion derived in previous part. And the Bragg frequency in bistatic HF surface wave radar could be calculated by

$$\omega_B = \sqrt{2kg\cos(\phi/2)} \tag{11}$$

where ϕ indicates the bistatic angle.

Intuitively, we try to generate a similar expression with (11). Therefore, an approximate formula (12) is given by analogy. However, albeit with the unity in form, the calculation error still exists. Since the relative error between (10) and (12) is small enough to be ignored, (12) is reasonable to be treated as the formula calculating the Bragg scattering frequency for most circumstance.

$$\omega_H \approx \sqrt{2kg\cos(\phi_H/2)} \tag{12}$$

where $\phi_H = 2\arctan(\dfrac{\sin\theta_r}{a/c - \cos\theta_r})$. The parameter a and c can be calculated through (5a) – (5b).

3. Analysis of Ionospheric Effect on the Clutter Resolution Cell

3.1 Effect of Ionosphere Dispersion on the Clutter Resolution Cell

It is well known that the clutter resolution cell is determined by the radar range resolution and azimuthal angle resolution, simultaneously. As far as the ionosphere influence is concerned, we emphasize on its distortion on the radar range resolution caused by the ionosphere dispersion profile. And the azimuthal angle resolution is not the focus of this work, since it is determined primarily by the aperture of the receiving array [13].

3.1.1 Analytical Expression of the Ionosphere Dispersion Transfer Function

Generally, the radar range resolution is usually determined by the waveform output of matching filter, which could be expressed as [15]

$$\rho(t) = \frac{1}{2\pi}\int M_r(j\omega) M_0^*(j\omega)\exp(j\omega t)d\omega . \tag{13}$$

According to (13), $M_r(j\omega)$ is the spectrum of the received signal and $M_0^*(j\omega)$ is the complex conjugate of the spectrum of the transmitted signal. On account of ionosphere dispersion, the received signal $m_r(t)$ should be written as the convolution output of the ionosphere dispersion transfer function $g(t)$ and $m(t)$ viz.

$$m_r(t) = \int_{-\infty}^{\infty} m(t-\tau)g(\tau)d\tau . \tag{14}$$

As for the dispersion transfer function, Lundborg [14] has yielded the ionospheric weighing function expressing the ionosphere dispersion causing the distortion of the pulse shape by (16), which forms a Fourier transform pair with (15).

	E Layer			F_1 Layer			F_2 Layer		
Parameters	$f_{cE}(MHz)$	$h_{mE}(km)$	$y_{mE}(km)$	$f_{cF_1}(MHz)$	$h_{mF_1}(km)$	$y_{mF_1}(km)$	$f_{cF_2}(MHz)$	$h_{mF_2}(km)$	$y_{mF_2}(km)$
	4.1	85	19	6	125	60	11	200	120
t_1	t_{1E}	0.10~1.03		$t_{1F_{1L}}$	0.17~3.11		$t_{1F_{2L}}$	0.20~6.14	
$\times 10^{-6} s$	—	—	—	$t_{1F_{1H}}$	18.30~24.56		$t_{1F_{2H}}$	17.58~24.56	

Tab. 1. Range of dispersive coefficient corresponding to each layer (the ground distance D = 2000 km).

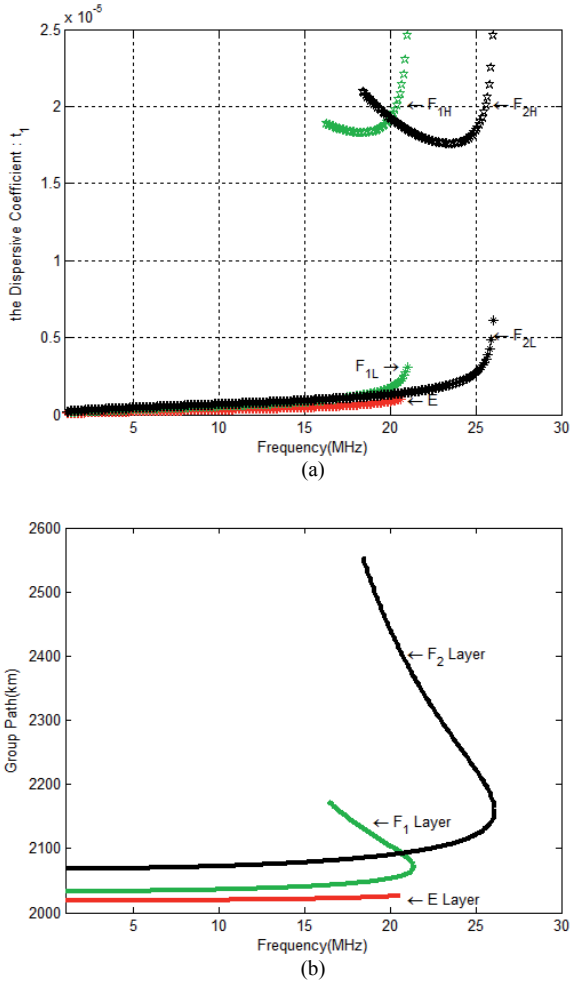

Fig. 4. Frequency variation of the (a) dispersive coefficient and (b) group path in a quasi-parabolic model for each ionosphere layer at the ground distance of 2000 km.

$$g(t) = t_1^{-1} \exp(-\pi i / 4 + \pi i t^2 / t_1^2), \tag{15}$$

$$G(\omega) = \mathcal{F}\left(g(t)\right) = \exp(-\pi i \omega^2 / f_1^2) \tag{16}$$

where t_1 is defined as the dispersive coefficient and $f_1 = 1 / t_1$ is called as the dispersive bandwidth. According to (16), it is easy to observe that the ionosphere dispersion function acts somewhat like a low pass filter in the frequency domain. And, as the unique parameter, the dispersive coefficient t_1 determines the scale of dispersive bandwidth essentially and therefore influences the extent of band pass filtering modulation on the signal envelope indirectly in accordance with (14).

Afterwards, an analytical expression to calculate t_1 under the assumption that the ionosphere is spherical stratified and the electron density of ionosphere obeys the quasi-parabolic model has been derived (see Appendix A). The reason why we choose such conditions is as follows:

- With regard of the detection over the horizon, one hop is usually more than hundreds of kilometers, making the assumption of plane stratified ionosphere structure untenable.
- Compared with the parabolic model adopted in [14], the quasi-parabolic model is an improved one with the introduction of a modified factor. Besides, it is much more appropriate to describe the ionospheric characteristic with the single layer structure.

Based on the formula derived in the Appendix A, Fig. 4 illustrates t_1 and the group path corresponding to E layer, F_1 layer and F_2 layer respectively versus different operating frequency. And the numerical calculation results are recorded in Tab. 1, where the first three parameters in each column indicate the critical frequency f_c, the distance between the bottom of ionosphere and the ground h_m and the ionosphere half thickness y_m respectively.

Furthermore, combined with the numerical calculation results, the property of the ionosphere dispersion could be boiled down to as follows: (1) the bandwidth for the low pass filter commonly ranges from hundreds of kilohertz to several megahertz; (2) In terms of F_1 and F_2 layers, as the transmitting frequency increases, there are generally two dispersive coefficient values corresponding to the high ray and low ray respectively. And the one with regard to the high ray exceeds that for the low ray; (3) As for each layer, the magnitude of dispersive coefficient value follows $F_2 > F_1 > E$.

3.1.2 Effect of Ionosphere Dispersion on Calculating the Area of Clutter Resolution Cell in Reality

According to Fig.4 (b), it is easy to observe that, as the frequency increases, there are generally two different values of group path, when the ground distance is fixed. And we call this the occurrence of multi-path in a single layer illustrated in Fig. 5.

One of the major influence triggered by multi-path propagation could be attributed to the pulse mixing due to the overlap of the convolution output of the high ray dispersion transfer function and the low ray one. Besides,

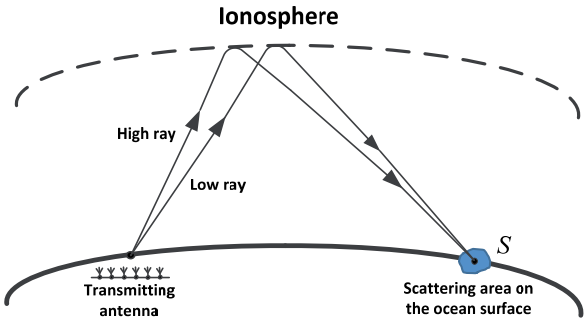

Fig. 5. A sketch map for the multi-path propagation including the high ray mode and low ray mode in a single layer.

combined with the filtering property of the ionosphere dispersive transfer function explicated in the previous section, the final signal $S_r(t)$ received by the receiver is a compound result imposed by the ionospheric band pass filtering and pulse mixing. And such modulating process could be expressed as

$$S_r(t) = \int e(t-\tau) g_L(\tau) d\tau + \int e(t-\tau) g_H(\tau) d\tau \,. \quad (17)$$

To explain this, Fig. 6(a) simulates the convolution output for a Gaussian narrow pulse reflecting from the F_1 layer. The relationship of bandwidth between $e(t)$, $g_H(t)$, and $g_L(t)$ satisfies as: $B_{wH} < B_{we} < B_{wL}$ (the subscript H and L indicate the high ray and low ray channel). Obviously, the echo reflecting from the low ray channel keeps nearly intact, while the envelope of the one corresponding to the high ray distorts seriously as B_{we} exceeds B_{wH} resulting in splitting and broadening of $e(t)$, which also deteriorates the envelope shape of final signal $S_r(t)$.

However, as for the HF radar, linear frequency modulated continuous wave (LFMCW) is usually implemented with a bandwidth of tens of kilohertz, which is far smaller than the ionosphere dispersive bandwidth. Therefore, the influence because of $g(t)$ filtering modulation would be nearly neglected, only remaining the envelop modulation impact due to pulse mixing. According to Fig. 6(b)–(c), the effect on the envelop modulation can be detected and confirmed both from the simulation and the experimental echo envelope.

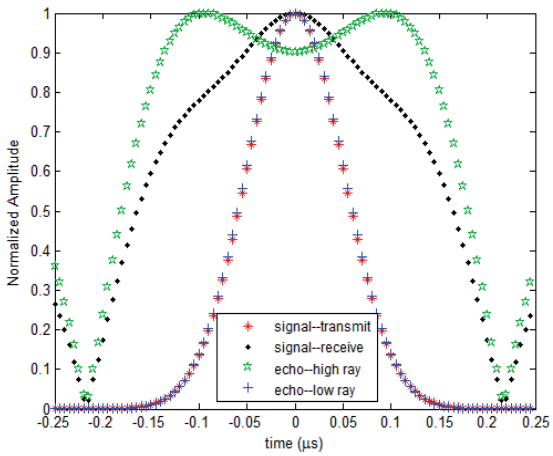

(a) The effect on Gaussian pulse propagation.

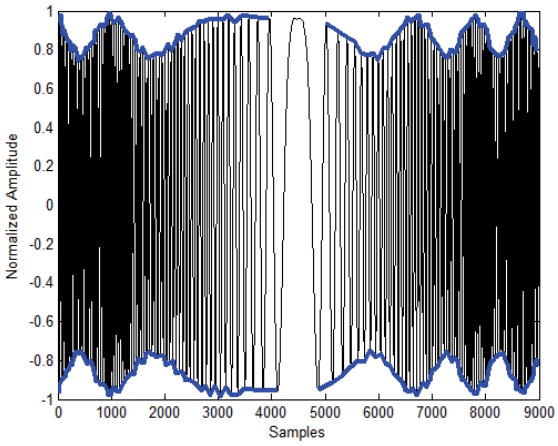

(b) The effect on narrow band LFMCW based on simulation result.

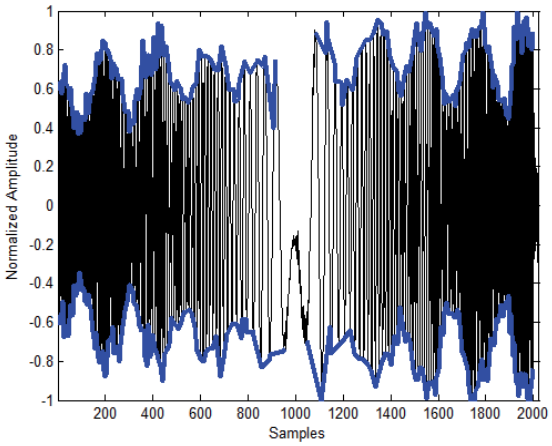

(c) The effect on narrow band LFMCW based on experiment result.

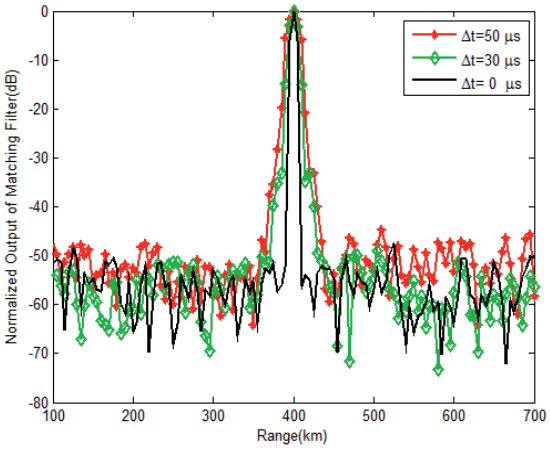

(d) Output of matching filter.

Fig. 6. The effect of ionosphere dispersion on pulse propagation and the output of matching filter.

Essentially, the envelop modulation would lead to the peak spreading of the output after range processing by (13). To illustrate this, Fig. 6(d) gives a number of results corresponding to different time delay Δt ($\Delta t = (P_H - P_L) / c_v$ indicates the time difference between the high ray and low ray path, and c_v is the velocity of light). Actually, the time interval between each discrete sample after range processing is $\tau = 1 / B_w$ (the derivation is given in Appendix B).

Based on which, it is reasonable to infer that as long as Δt is smaller than τ, the echoes scattered originally from two adjacent range bins would be folded into one, which is equivalent to the expansion of the clutter resolution cell area. This result is also in accordance with peak broadening of $\rho(t)$. Therefore, the area of such enlarged clutter resolution cell illuminated by the receiving beam with the azimuthal angle resolution $\Delta\theta$ at a distance of R could be calculated by

$$\Delta S = \frac{c_v(\tau + \Delta t)\Delta\theta R}{2}. \tag{18}$$

3.2 Limits of Ionosphere on the Clutter Resolution Cell

The ionosphere causes radar pulses with a certain bandwidth to spread in ground range due to the ionization profile [16]. If this spreading range exceeds the radar range resolution, then the performance is degraded. In addition, the azimuthal angle resolution is also restricted by the nature of fine-scale irregularities in the ionosphere plasma density [17]. On account of these, the ionosphere is bound to place a practical limit on the radar waveform bandwidth and azimuthal angle resolution in order to avoid worsening the radar detection performance. Recently, the formula to describe and calculate the influence quantitatively has been studied by Li [18]

$$\Delta B_{\lim} = \sqrt{\pi c_v \omega_{p0}^2 / (2\omega z_0 \sin(2\beta))}, \tag{19}$$

$$\Delta\theta_{\lim} = \frac{2\sqrt{2L\kappa_0 \left\langle n_1^2 \right\rangle (r_e \lambda \sec\beta)^2}}{k} \tag{20}$$

where r_e is the classical electron radius (2.8×10^{-15} m), $\left\langle n_1^2 \right\rangle$ is the mean square density of the plasma irregularities, L is the horizontal distance travelling in the ionosphere, κ_0 is the outer scale length of irregularities, ω_{p0} is the plasma frequency, z_0 is the distance between the ground and the bottom of ionosphere, β is the elevation angle, ω is the radar operating angular frequency, c_v is the velocity of light. Hence, based on (19)–(20), the area of the limited clutter resolution cell at a distance of R is given by

$$\begin{aligned}\Delta S_{\lim} &= \frac{R\Delta\theta_{\lim} c_v}{2\Delta B_{\lim}} = \frac{Rc_v\sqrt{2L\kappa_0 \left\langle n_1^2 \right\rangle (r_e\lambda\sec\beta)^2}}{k\sqrt{\pi c_v\omega_{p0}^2/(2\omega z_0\sin(2\beta))}} \\ &= \frac{2Rc_v}{k}\sqrt{\frac{L\kappa_0 \left\langle n_1^2 \right\rangle (r_e\lambda\sec\beta)^2 \omega z_0 \sin(2\beta)}{\pi c_v \omega_{p0}^2}}\end{aligned} \tag{21}$$

In fact, the limit of ionosphere on the resolution cell discussed here mainly focuses on quantitatively calculating the area of the resolution cell, within which the backscattered sea clutter echo could be regarded as homogeneous and relevant so as to provide a reference on dividing the actual clutter resolution cell.

3.3 Comparison between $\Delta S_{\lim}$ and ΔS

Previously, the influence on the clutter resolution cell triggered by the ionosphere has been deeply discussed. Afterwards, we would put a stress on the comparison between the limit area $\Delta S_{\lim}$ and the one ΔS in reality. Tab. 2 provides a series of numeral results to explain this. Simulation parameters are selected as follows: the baseline $D_0 = 800$ km, $\omega_{p0}/(2\pi) = 5$ MHz, $z_0 = 130$ km, $L = 600$ km, $\left\langle n_1^2 \right\rangle = 10^{19}\text{m}^{-6}$, $\kappa_0 = 10^{-4}$/m, $B_w = 30$ kHz, the half thickness of the ionosphere $y_m = 60$ km and the distance between the earth center and the ionospheric layer corresponding to the maximum electron density $r_m = r_b + y_m = 6860$ km. For the sake of simplicity, we denote $\delta = \Delta S / \Delta S_{\lim}$.

According to Tab. 2, the relationship between $\Delta S_{\lim}$ and ΔS could be summed as: (1) the limit on the bandwidth and the azimuthal angle resolution is restricted with each other; (2) δ is generally proportional to the radar operating frequency, the time delay Δt and θ_r.

f (MHz)	R = 200 km, $\theta_r = 150^\circ$						
	$\Delta B_{\lim}$ (kHz)	$\Delta\theta_{\lim}$ (°)	$\Delta S_{\lim}$ (km × km)	Δt (μs)	$\Delta B_{\lim} / B_w$	$\Delta\theta / \Delta\theta_{\lim}$	δ
5	262.9	7.3	14.6	0	8.8	1.4	12.0
8	205.3	2.9	7.4	0	6.8	3.5	23.7
13	155.2	1.2	4.1	0.2	5.1	8.8	42.1

(a) δ versus different operating frequency for a given detection clutter cell.

θ_r (°)	d = 1200 km, f = 6 MHz						
	$\Delta B_{\lim}$ (kHz)	$\Delta\theta_{\lim}$ (°)	$\Delta S_{\lim}$ (km × km)	Δt (μs)	$\Delta B_{\lim} / B_w$	$\Delta\theta / \Delta\theta_{\lim}$	δ
30	188.1	6.7	30.2	0	6.3	1.5	9.4
90	219.4	5.4	9.2	0	7.3	1.8	13.5
150	227.4	5.3	5.5	0	7.6	1.9	14.4

(b) δ versus different clutter cells for a given operating frequency.

Tab. 2. Comparison result between $\Delta S_{\lim}$ and ΔS.

4. First Order Sea Clutter Cross Section Simulation and Experiment Results

4.1 A Method to Simulate the First Order Sea Clutter Cross Section

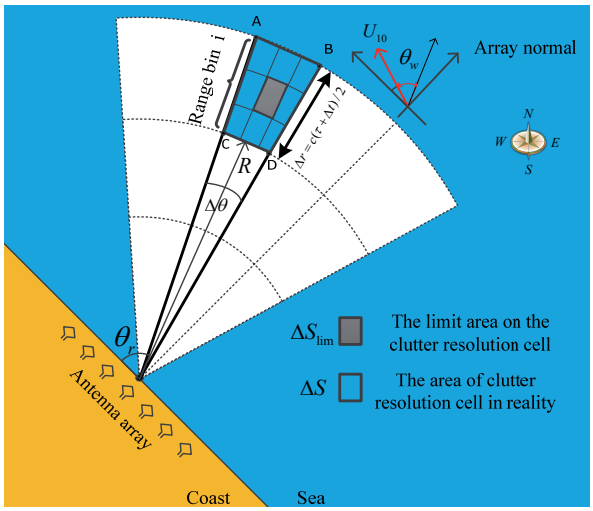

Fig. 7. Illustration for the relationship between $\Delta S_{\lim}$ and ΔS.

The first order sea clutter cross section applied in the bistatic surface wave has been proposed by Walsh and Gill [12], [19]

$$\sigma_1(\omega_d)=2^4\pi k^2\sum_{m=\pm1}S(m\boldsymbol{K})\frac{K_d^{5/2}\cos\phi_0}{\sqrt{g}}\Delta R \times Sa^2\left[\frac{\Delta R}{2}\left(\frac{K_d}{\cos\phi_0}-2k\right)\right] \tag{22}$$

where $K_d=\omega_d^2/g$, ω_d is the Doppler angular frequency, $\phi_0=\phi_H/2$ is the half bistatic angle, ΔR indicates the range resolution, $Sa(\cdot)$ is the sinc function. The directional wave height spectrum $S(m\boldsymbol{K})$ considered here is the product of non-directional P-M spectrum and the standard form of the normalized directional distribution [12].

Given the following mathematic relationship in (23) and (24)

$$\Delta R\times Sa^2\left[\frac{\Delta R}{2}\left(\frac{K_d}{\cos\phi_0}-2k\right)\right]=2\cos\phi_0\times\frac{\Delta R}{2\cos\phi_0}\times Sa^2\left[\frac{\Delta R}{2\cos\phi_0}(K_d-2k\cos\phi_0)\right] \tag{23}$$

$$\lim_{M\to\infty}MSa^2(Mx)=\pi\delta(x). \tag{24}$$

Equation (22) could be simplified as

$$\sigma_1(\omega_d)=2^4\pi k^2\sum_{m=\pm1}S(\mathrm{m}\boldsymbol{K})\left[2kg\cos\phi_0\right]^{5/2}\frac{\cos\phi_0}{\sqrt{g}} \times\frac{2\pi g\cos\phi_0}{2\sqrt{2kg\cos\phi_0}}\delta\left(\omega_d+m\sqrt{2kg\cos\phi_0}\right) =2^6\pi^2k^4\cos^4\phi_0\times \sum_{m=\pm1}S(\mathrm{m}\boldsymbol{K})\delta\left(\omega_d+m\sqrt{2kg\cos\phi_0}\right) \tag{25}$$

Judging from the derivation process in [19], equation (25) is appropriate to be applied to calculate the radar cross section for the clutter within $\Delta S_{\lim}$, because the clutter distributed within $\Delta S_{\lim}$ is equipped with the highest correlation. Hence, based on the analysis in Section 3, as well as the relationship illustrated in Fig. 7, a much more accurate model may be generated after taking $\Delta S_{\lim}$ as the standard to divide ΔS. The dividing criterion refers to the relative scale of $B_w/\Delta B_{\lim}$ and $\Delta\theta/\Delta\theta_{\lim}$. By virtue of such manipulation, we suppose that the sea clutter distributed in each unit could be approximately treated as independent and identically distributed (i.i.d); thus, the mean cross section $\bar{\sigma}_1(\omega_d)$ corresponding to ΔS could be obtained by

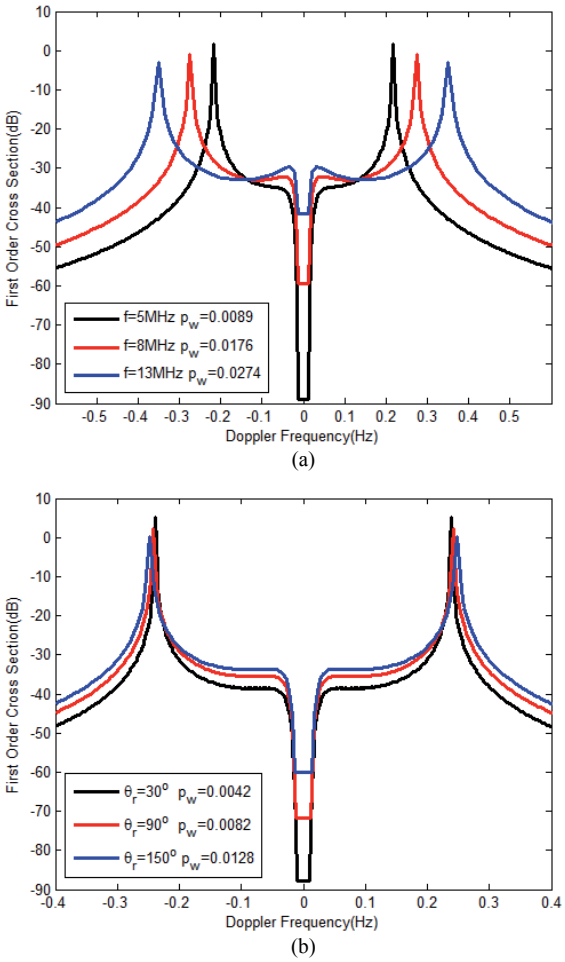

Fig. 8. The first order sea clutter cross section variance of operating frequency and θ_r in accordance with results of Tab. 2.

$$\bar{\sigma}_1(\omega_d) = \frac{\sum_{n=1}^{N} \sigma_1(\omega_d)_n \cdot \Delta S_{\lim}(n)}{\sum_{n=1}^{N} \Delta S_{\lim}(n)} \tag{26}$$

where N stands for the total number of divided clutter cells. Besides, in order to describe the spectral pattern quantitatively, the equivalent spectral width of the first order line is defined as

$$P_w = \int_{f_H-\Delta}^{f_H+\Delta} P(f)df \,/\, P_0 \tag{27}$$

where f_H is the Doppler frequency of the largest Bragg line. $P(f)$ is the spectral density and Δ is the theoretical Doppler shift of the Bragg line (Δ applied in this paper is equal to the radar Doppler resolution), P_0 indicates all the energy.

Furthermore, simulation has been conducted to explicate the variety of first order sea clutter cross section after taking account of the clutter division. The simulation parameters selected here are in consistent with the ones applied in Tab. 2. Combined with (25) and (26), Fig. 8 presents a straightforward variance of the first order cross section. Meanwhile, allowing for the fact that system timing effects as well as surface fluctuations and noise will, in practice, provide a smoothing effect. Therefore, the result in Fig. 8 has been simulated by convolving the cross section with a Hamming window in consistence with [19]. According to Fig. 8, the amplitude and spectral width are changing with different operating and detection parameters. Essentially, such phenomenon could be explained by the relative scale between $\Delta S_{\lim}$ and ΔS. That is to say, as long as ΔS exceeds the limit scale on the resolution cell, the clutter distributed in the area surpassing $\Delta S_{\lim}$ would be superimposed and overlapped. And for such a big area ΔS, the deteriorating correlation of the sea clutter is bound to result in spectral peak energy spreading to adjacent Doppler bins.

4.2 Simulation and Experiment Results

The experiment data was obtained from the newly-developed HF sky-surface wave experimental platform in HIT, which is illustrated in Fig. 9 (a)–(b). The basic operating parameters applied in this system are: the operating frequency f = 15 MHz, the baseline length D_0 = 800 km, the bandwidth B_w =40 kHz, the pulse repetition period is 20 ms, coherent integration time (CIT) CIT = 51.20 s, the normal direction of the receiving array is 58° from north to west and the element number of the uniform linear array is eight. The reflection happens at F_2 layer. The sea state is 3 measured in Douglas offing state grade [13]. Fig.9 (c)–(d) give us an ad hoc image after taking the manipulation of range and Doppler processing. It is well to be spotted that the spectral pattern, especially the spectral width, varies with different receiving direction (θ_r) and range bins, therefore exhibiting a spatial variance property [7], [20].

In conjunction with the experiment result, the according simulation has been conducted to testify the validity of the method proposed in calculating the cross section of the first order sea clutter in Fig. 10. The simulation parameters applied herein are in accordance with those for the experiment and the calculation results of δ equal to 32, 65, 58 and 40 respectively. Simultaneously, the spectral width P_w is also calculated to contrast the discrepancy between each spectral pattern. According to Fig. 10, several straightforward conclusions could be yielded:

- Given a selected clutter cell, P_w is proportional to the array antenna receiving direction, indicating the occurrence of spectrum spreading. Besides, as for different range bins illuminated within the same beam, the clutter echo spectrum corresponding to the far range bin is sharpen in contrast with the ones from the range bin adjacent to the receiver. Albeit with the variance of θ_w (the definition is illustrated in Fig. 7) in each simulation, it merely affects the relative magnitude between the negative and positive Bragg peaks, but not the spectral width.
- The characteristic of the first order sea clutter spectral pattern is in accordance with the calculation result of δ. Such consistency also confirms the effectiveness and validity of clutter resolution cell division when calculating the actual sea clutter cross section.

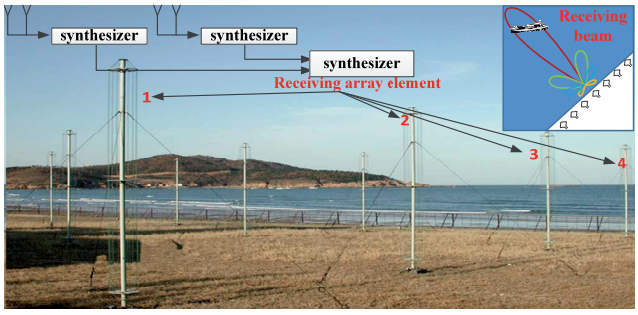

(a) An actual layout of radar receiving antenna array.

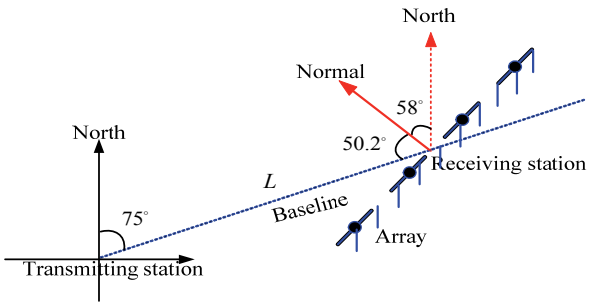

(b) The array geometric layout of the transmitting and receiving stations.

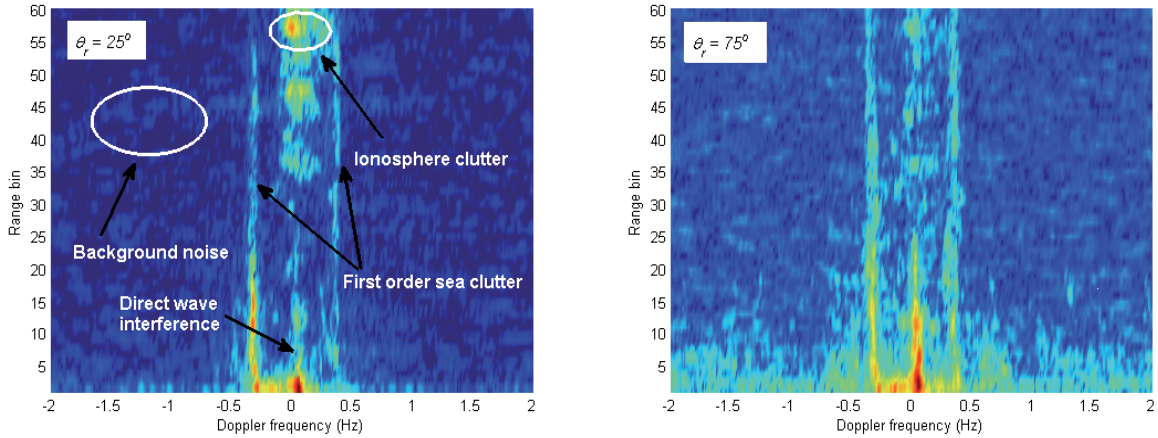

(c) The range and Doppler image with θ_r=25° .

(d) The range and Doppler image with θ_r=75° .

Fig. 9. Illustration of the experimental platform and range-Doppler processing result of the experiment data versus different receiving direction θ_r .

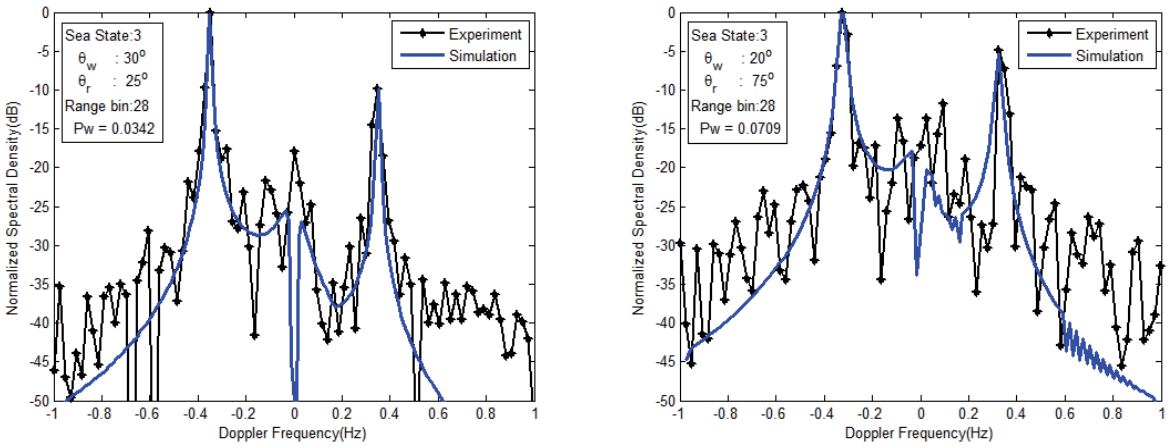

(a) Spectral pattern variance versus different receiving direction θ_r .

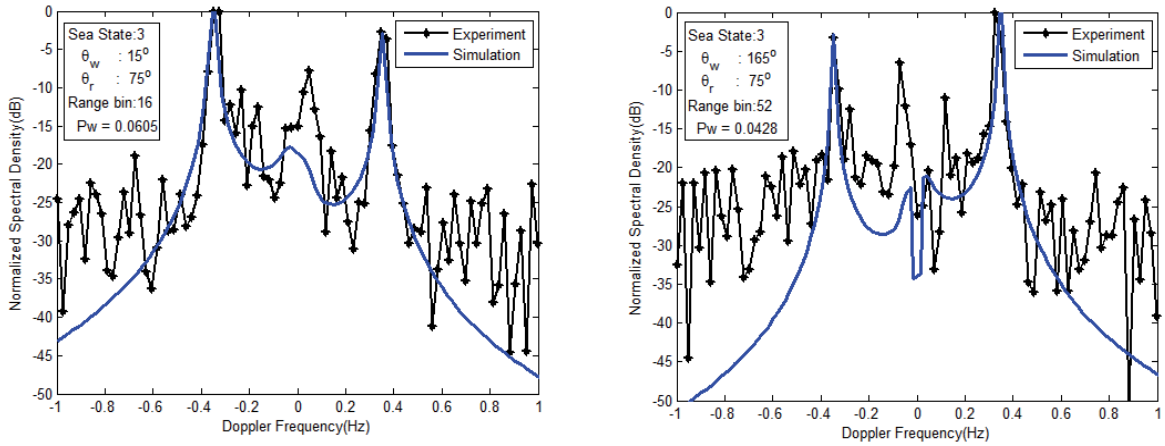

(b) Spectral pattern variance versus different range bins.

Fig. 10. Comparison between the simulation result and the normalized sea clutter spectral density obtained from the experiment data.

5. Conclusion

In this paper, with regard to the ad hoc hybrid sky-surface propagation mode, some elementary problems have been discussed and studied deeply and extensively.

The spatial geometry distribution of the first order sea clutter could be depicted as an ellipse for a fixed time delay under a relatively ideal condition. Based on which, the Bragg scattering frequency is derived. It can be recognized that the results are similar to those derived in the bistatic surface wave radar, but a redefinition is supposed to be conducted on some parameters, especially the bistatic angle.

Subsequently, we explicate how the ionosphere dispersion impacts on the clutter resolution cell. Specifically, we have demonstrated that the property of the dispersion transfer function acts somewhat like a band pass filter. According to this property, the ionosphere dispersion has put forward a clear restriction on the radar operating frequency as well as some other detection parameters so as to avoid the distortion on the transmitting signal and the occurrence of multi-path travelling. On top of this, the limit of ionosphere on the clutter resolution cell has been discussed so as to recognize how big the size of clutter resolution cell could be treated as a unit area, so that the traditional first order sea clutter cross section model derived by Walsh and Gill [12], [19] can be used.

Eventually, a modified simulation method for the first order sea clutter cross section is derived and discussed. Through the simulation, we have demonstrated how the spectral width spreads versus different δ. According to the compared result between experiment and simulation, the clutter cell division appears to be imperative when regarding the coherence between adjacent clutter cells. Therefore, in the actual detection, some ad hoc restriction should be put to minimize the area of the clutter resolution cell as much as possible so as to avoid the spreading of the clutter spectrum, which may necessitate a radically different radar system design.

Acknowledgements

This work was supported by the National Natural Science Foundation Project grant (No.61471144) to China. The authors appreciate the help from the Institute of Electronic Engineering Technology in HIT for providing the experimental data.

References

[1] MELYANOVSKI, P. A., TOURGENEV, I. S. Bistatic HF radar for oceanography applications with the use of both ground and space waves. *Telecommunications and Radio Engineering*, 1997, vol. 51, no. 2-3, p. 73–79.

[2] ZHAO, Z.X., WAN, X.R., ZHANG, D.L., CHENG, F. An experimental study of HF passive bistatic radar via hybrid sky-surface wave mode. *IEEE Transactions on Antennas and Propagation*, 2013, vol. 61, no. 1, p. 415–424.

[3] JIANG, W., DENG, W.B., YANG, Q. Analyses of sea clutter for HF over the horizon hybrid sky-surface wave radar. *Journal of Electronics & Information Technology*, 2011, vol. 33, no. 8, p. 1786–1791.

[4] LI, Y.J., WEI, Y.S. Analysis of first-order sea clutter spectrum characteristics for HF sky-surface wave radar. In *2013 International Conference on Radar*. Australia, 2013, p. 368–373.

[5] ANDRIĆ, M., BUJAKOVIĆ, D., BONDŽULIĆ, B., SIMIĆ, S., ZRNIĆ, B. Analysis of radar Doppler signature from human data. *Radioengineering*, 2014, vol. 23, no. 1, p. 11–19.

[6] LI, Y.J., WEI, Y.S., ZHANG, C., SHANG, C., TANG, X.D. Influence of ionosphere on SCR of HF hybrid sky-surface wave radar. In *IET International Radar Conference*. Xi'an (China), 2013, p. 1–6.

[7] LI, Y.J., WEI, Y.S., XU, R.Q., CHU, T.Q., WANG, Z.Q. Space-time characteristics and experimental analysis of broadening first-order sea clutter in HF hybrid sky-surface wave radar. *Radioengineering*, 2014, vol. 23, no. 3, p. 831–841.

[8] RIDDOLLS, R. J. Ship detection performance of a high frequency hybrid sky-surface wave radar. *Defense R&D Canada-Ottawa*, 2007, p. 1-42.

[9] ZHU, Y.P., SHANG, C., LI, Y.J., A FBLP based method for suppressing sea clutter in HFSWR. In *International Symposium on Antennas and Propagation.* Nanjing (China), 2013, p. 1090–1093.

[10] HOU, C.Y., KE, G., SHI, T.G., WANG, Y.X. Study on the detectability of the sky-surface wave hybrid radar. *Journal of Applied Mathematics*, 2014, p. 1-10.

[11] BARRICK, D. E. First-order theory and analysis of MF/HF/VHF scatter form the sea. *IEEE Transactions on Antennas and Propagation*, 1972, vol. 20, no. 1, p. 2–10.

[12] WALSH, J., DAWE, B. J. Development of a model for the first order bistatic ocean clutter radar cross section for ground wave radars. *Northern Radar Systems Limited contract report for the Defense Research Establishment Ottawa*, 1994, p. 1-74.

[13] BARTON, D. *Modern Radar Systems Analysis*. Norwood: Artech House, 1987.

[14] LUNDBORG, B. Pulse propagation through a plane stratified ionosphere. *Journal of Atmospheric and Terrestrial Physics*, 1990, vol. 52, no. 9, p. 759–770.

[15] KRETOV, N. V., RYSHKINA, T. Y., FEDOROVA, L. V. Dispersive distortions of transionospheric broadband VHF signals. *Radio Science*, 1992, vol. 27, no. 4, p. 491–495.

[16] RIDDOLLS, R. J. Limits on the detection of low-Doppler targets by a high frequency hybrid sky surface wave radar system. In *2008 IEEE Radar Conference*, Rome (Italy), 2008, p. 1–4.

[17] RIDDOLLS, R. J. Detection of aircraft by high frequency sky wave radar under auroral clutter-limited conditions. *Defense R&D Canada-Ottawa*, 2008, p. 1–38.

[18] LI, Y.J., WEI, Y.S., XU, R.Q. Influence of ionosphere on resolution cell of HF hybrid sky-surface wave radar. In *Antennas and Propagation Society International Symposium (APSURSI)*. Orlando (USA), 2013, p. 1028–1029.

[19] GILL, E. The scattering of high frequency electromagnetic radiation from the ocean surface: An analysis based on a bistatic ground wave radar configuration. *PhD Thesis.* Faculty of Engineering and Applied Science, Memorial University of Newfoundland, 1999.

[20] LI, Y. J., WEI, Y.S., XU, R.Q., SHANG, C. Simulation analysis and experimentation study on sea clutter spectrum for high-frequency hybrid sky-surface wave propagation mode. *IET Radar Sonar and Navigation*, 2014, p. 1-14.(in press, doi: 10.1049/iet-rsn.2013.0289)

[21] CROFT, T., HOOGASIAN, H. Exact ray calculations in a quasi-parabolic ionosphere with no magnetic field. *Radio Science*, 1968, vol. 3, no. 1, p. 69.

Appendix

A. Derivation of the Dispersive Coefficient for a Spherical Stratified Ionosphere

In this section, we shall derive the explicit expression of the dispersive coefficient t_1 under the assumption that the ionosphere is spherical stratified and the electron density of ionosphere submits to the quasi-parabolic model. The Q-P model, a modified one by a slight modification of the parabolic model, is introduced by Croft and Hoogasian [21]. As in the case of quasi-parabolic model, the quasi-parabolic layer of semi-thickness y_m can be modeled as

$$f_p^2 = \frac{f_c^2}{f^2}\left[1-\left(\frac{r-r_m}{y_m}\right)^2\left(\frac{r_b}{r}\right)\right] \quad r_b \le r \le \frac{r_m r_b}{r_b - y_m}$$

$$f_p^2 = 0 \qquad \text{Elsewhere}$$

Here the critical frequency is related to the maximum electron density N_m and wavenumber k by $f_c = \sqrt{kN_m}$ .r_b is the distance between the bottom of ionosphere and the earth center; and r_m indicates the distance between the earth center and the ionospheric layer corresponding to the maximum electron density. Actually, the ionization rises from zero at $r = r_b$ at the base of the ionosphere to a peak value N_m at $r = r_m = r_b + y_m$.

The expressions for the ground distance D and the group path P for the quasi-parabolic layer are

$$P = 2(1-F^2/A)r_b \sin - 2r_0 \sin\beta - (BF/2A^{3/2})\ln(U/V^2),$$

$$D = 2r_0\left\{(r-\beta) - \frac{Fr_0\cos\beta}{2\sqrt{C}}\times \left(\ln(U) - \ln\left(4C(F\sin\gamma + \frac{1}{r_b}\sqrt{C} + \frac{B}{2\sqrt{C}})^2\right)\right)\right\}$$

where $F = f/f_c$, $\gamma = \cos^{-1}\left[(r_0/r_b)\cos\beta\right]$, $U = B^2 - 4AC$, $A = F^2 - 1 + (r_b/y_m)^2$, $C = \left(r_b r_m / y_m\right)^2 - F^2 r_0^2\cos^2\beta$, $V = 2Ar_b + B + 2r_b FA^{1/2}\sin\gamma$ and $B = -2r_m r_b^2 / y_m^2$.

In our analysis, the dispersive coefficient t_1 is primarily determined by the frequency derivative of the group path.

$$t_1 = \sqrt{\frac{1}{c_v}\cdot\frac{dP}{df}} = \sqrt{\frac{1}{c_v f_c}\left(\frac{\partial P}{\partial F} - \frac{\partial P}{\partial\beta}\frac{\partial D}{\partial F}\Big/\frac{\partial D}{\partial\beta}\right)}$$

where

$$\frac{\partial D}{\partial F} = \frac{r_0^2\cos\beta}{C^{1/2}}\left[\left(\frac{F\dot{C}_F}{2C} - 1\right)\Phi + 4F\frac{\dot{A}_F C + A\dot{C}_F}{B^2 - 4AC} + 2F\frac{\dot{C}_F r_b F\sin\gamma + 2Cr_b\sin\gamma + 2\dot{C}_F C^{1/2}}{C^{1/2}\left(2C^{1/2}r_b F\sin\gamma + 2C + Br_b\right)}\right] \tag{A-1}$$

$$\frac{\partial D}{\partial\beta} = 2r_0(\dot{r}_\beta - 1) + \frac{Fr_0^2\cos\beta}{C^{1/2}}\left[(\frac{\dot{C}_\beta}{2C} + \tan\beta)\Phi + \frac{4A\dot{C}_\beta}{B^2 - 4AC} + 2\frac{\dot{C}_\beta r_b F\sin\gamma + 2\dot{r}_\beta C r_b F\cos\gamma + 2\dot{C}_\beta C^{1/2}}{C^{1/2}\left(2C^{1/2}r_b F\sin\gamma + 2C + Br_b\right)}\right] \tag{A-2}$$

$$\frac{\partial P}{\partial F} = \frac{2F^2 r_b\sin\gamma}{A^2}\dot{A}_F - \frac{4r_b\sin\gamma F}{A} - \left(\frac{BW}{2A^{3/2}} - \frac{3BFW}{4A^{5/2}}\dot{A}_F + \frac{BF}{2A^{3/2}}\dot{W}_F\right) \tag{A-3}$$

$$\frac{\partial P}{\partial\beta} = \left(2 - \frac{2F^2}{A}\right)r_b\dot{r}_\beta\cos\gamma r_b\dot{r}_\beta\cos\gamma - 2r_0\cos\beta - \frac{BF}{2A^{3/2}}\dot{W}_\beta \tag{A-4}$$

And the relevant parameters in (A-1) – (A-4) are

$$\dot{W}_F = -\frac{4\dot{A}_F C + 4A\dot{C}_F}{B^2 - 4AC} - 2\times\frac{2\dot{A}_F r_b + 2r_b A^{1/2}\sin\gamma + r_b FA^{-1/2}\dot{A}_F\sin\gamma}{V}$$

$$\dot{W}_\beta = -\left(4\frac{A\dot{C}_\beta}{B^2 - 4AC} + 2\frac{2r_b FA^{1/2}\dot{r}_\beta\cos\gamma}{V}\right),$$

$$\dot{A}_F = 2F\ ,\quad \dot{C}_F = -2Fr_0^2\cos^2\beta\ ,\quad \dot{r}_\beta = \frac{r_0\sin\beta}{\sqrt{r_b^2 - r_0^2\cos^2\beta}},$$

$$W = \ln\frac{U}{V^2} = \ln\frac{B^2 - 4AC}{\left(2Ar_b + B + 2r_b FA^{1/2}\sin\gamma\right)^2},$$

$$\dot{C}_\beta = F^2 r_0^2\sin 2\beta\ ,\quad \Phi = \ln\frac{\left(B^2 - 4AC\right)r_b^2}{\left(2C^{1/2}r_b F\sin\gamma + 2C + Br_b\right)^2}.$$

B. Derivation of Time Interval Corresponding to a Range Bin after Range Processing

We take the LFMCW as the emission signal and thus we have:

$$S_t(t) = \cos\left[2\pi\left(ft + K(t-nT)^2/2\right)\right].$$

The echo signal could be expressed as:

$$S_r(t) = \cos\left[2\pi(f(t-\tau_d) + K(t-nT-\tau_d)^2/2)\right]$$

where f is the radar operating frequency, $K = B_w/T$ is the modulation rate, $\tau_d = 2(R_0 - v_r t)/c_v$ is the time delay determined by the position of the target, T is the modulation period, $n = -\infty,\cdots,0,1,\cdots,+\infty$ is the index of modulation period. And the phase output $\psi_b(t)$ after mixing with the local oscillator is

$$\begin{aligned}\psi_b(t) &= \psi_t(t) - \psi_r(t)\\ &= 2\pi\left[ft + \frac{K}{2}(t-nT)^2 - f(t-\tau_d) - \frac{K}{2}(t-nT-\tau_d)^2\right]\\ &= 2\pi\left[f\tau_d + \frac{K}{2}\tau_d(2t-2nT-\tau_d)\right]\\ &= 2\pi\left[f\cdot 2\frac{R_0 - v_r t}{c_v} + K\cdot 2\frac{R_0}{c_v}(t-nT) - \frac{K}{2}{\tau_d}^2\right]\\ &= 2\pi\left[\frac{2fR_0}{c_v} - f_d nT + (f_R - f_d)(t-nT) - \frac{K}{2}{\tau_d}^2\right]\end{aligned}$$

Here we just focus on the frequency f_R corresponding to the range of the target:

$$f_R = 2KR_0/c_v = Kt_d\ .$$

Hence, after the stretch processing, the time interval is:

$$\tau = \Delta t_d = \frac{1}{K}\Delta f_R = \frac{1}{K\times T} = \frac{1}{B_w}$$

where Δf_R is determined by the Doppler resolution.

About Authors…

Yongpeng ZHU was born in Heilongjiang, China. He received the M.S. degree from HIT in 2014. He is currently working on the Doctorate degree in Information and Communication Engineering from HIT. His research interests include the fields of signal processing and radar system simulation in HF OTH radar.

Yinsheng WEI was born in 1974. He received his M.S. and Ph.D. degrees in Communication and Information Systems from Harbin Institute of Technology (HIT) in 1998 and 2002, respectively. And then, he joined the Department of Electronics Engineering in HIT as a lecturer, and became a professor in 2011. He is a member of IEEE AES, and a senior member of CIE. His main researches include in radar signal processing and radar system analysis and simulation.

Yajun LI was born in 1983. He received the M.S. degree from Harbin Engineering University in Information and Communication Engineering in 2011. He is now a PhD student of School of Electronics and Information Engineering at Harbin Institute of Technology, China. His current research interests include space-time adaptive processing, suppression of sea clutter, and HF radar system simulation.